Dalton Transactions

ROYAL SOCIETY OF CHEMISTRY

PAPER

View Article Online
View Journal | View Issue

Cite this: *Dalton Trans.*, 2025, **54**, 8956

Phosphine-assisted synthesis of a nanostructured iridium catalyst for acceptorless dehydrogenation of alcohols and chemoselective hydrogenation of nitroarenes†

Jyotishma Baruah and Pankaj Das *

Ligand-assisted synthesis of noble metal nanoparticles has gained significant recent interest in the field of heterogeneous catalysis. In line with this, herein, we report the synthesis of a nanostructured iridium catalyst supported on silica *via* a one-pot wet chemical approach by treating $IrCl_3$ with commercially available phosphine-functionalized silica gel, without the use of an external reducing or stabilizing agent. The phosphine ligand attached to silica plays the dual role of stabilizing and reducing agents. High-resolution transmission electron microscopy (HR-TEM) analysis revealed the formation of uniformly sized iridium nanoparticles (Ir NPs ~2 nm), consistently distributed throughout the silica surface without showing any signs of agglomeration. The nanomaterial was also characterized by other techniques such as SEM-EDX, XRD, ICP-AES, and XPS. To test the catalytic potential of the iridium-based material, oxidant-free dehydrogenation of primary alcohols to carboxylic acids, with concomitant liberation of two equivalents of molecular hydrogen, was chosen as the benchmark reaction. A range of primary alcohols, including usually less reactive aliphatic alcohols, can be converted to their corresponding carboxylates/acids in high yields, demonstrating excellent efficacy and a broad substrate scope, better than the state-of-the-art Ir-based heterogeneous catalysts reported to date for this transformation. In addition, the Ir-based nanomaterial was also explored as a catalyst for chemoselective hydrogenation of nitroarenes to aminoarenes. Moderate to excellent yields of the desired products were obtained with a diverse range of substrates. For both catalytic reactions, the catalyst was found to be recyclable for at least eight consecutive runs without significantly compromising yields.

Received 13th March 2025,
Accepted 29th April 2025

DOI: 10.1039/d5dt00607d

rsc.li/dalton

Introduction

Phosphines are among the most influential ligands in homogeneous catalysis due to their uniqueness in tuning the activity and selectivity of a catalytic system.[1,2] However, these homogeneous systems traditionally suffer from some inherent drawbacks, such as challenging catalyst separation, handling inconvenience, recycling difficulty, *etc.*, and hence are not sustainable from both economic and ecological perspectives. Consequently, many efforts are being made to expand the scope of phosphines from homogeneous to heterogeneous systems, including their use as surface-capping ligands in the synthesis of metal nanoparticles (MNPs), mostly with noble metals such as Ru,[3] Rh,[4,5] and Pd.[6,7] It may be noted that, in the past few years, surface-ligand-assisted synthesis of MNPs has marked a significant breakthrough in the realm of heterogeneous catalysis, paving the way for unprecedented advancements in this field.[8–10] Typically, the catalytic efficiency of such materials depends on several factors, such as the nature of the ligand, the nature of the support, the strength of the metal–ligand interfacial interactions, control over metal–particle dispersion, sizes and shapes of the nanoparticles, *etc.*[8–11] Usually, a strong metal–ligand interaction offers better control over morphology (sizes and shapes) and develops a strong interfacial connection that can significantly influence the catalytic efficiency.[9,12–14] On the other hand, a weak metal–ligand interaction may not provide enough stability over the growth and aggregation of the NPs. It can also result in the leaching of the metal species from the support during catalysis, causing poor recycling efficacy.

In the past few years, apart from phosphines, other ligands like carboxylates,[15,16] N-heterocyclic carbenes (NHCs),[17,18]

Department of Chemistry, Dibrugarh University, Dibrugarh-786004, Assam, India. E-mail: pankajdas@dibru.ac.in

†Electronic supplementary information (ESI) available: Figures illustrating SEM-EDX (fresh and recycled); recycled HR-TEM and P-XRD; catalyst optimization tables for the AD reaction of alcohols and nitroarene hydrogenation; ESI-MS spectra; ^1H and ^{13}C NMR spectra of almost all the products. See DOI: https://doi.org/10.1039/d5dt00607d

amines,[19,20] thiols,[21,22] *etc*., have also been exploited as surface-capping ligands for stabilizing MNPs. The binding affinity of such ligands is often correlated to Pearson's "hard–soft acid–base" concept.[13] For example, surface-capping carboxylates/amines, which are usually considered as hard/borderline bases, exert poor stabilization effects with soft metals like Ir or Pd.[23] In contrast, phosphines or thiols, due to their softness, behave as better stabilizing ligands for noble metals with applications in many catalytic organic transformations.[24] It may be noted that phosphine was used for the first time as a stabilizing ligand for MNP synthesis (AuNPs) about four decades ago.[25] Since then, several groups have been utilizing phosphines as surface-capping ligands for the synthesis of MNPs composed of Au,[26,27] Pd,[6,7,28] Ru,[3] and Rh,[5,29] and applied those MNPs in a range of catalytic applications. Typically, MNPs are synthesized from their corresponding salts *via* a chemical reduction method using external reducing agents like $NaBH_4$[30,31] and N_2H_4,[11] either with or without the presence of an external stabilizer, and the methods involve multiple steps for purification. However, there are a few instances where a surface-capping ligand like phosphine can play the dual role of a stabilizer and reducing agent (*in situ*), while synthesizing MNPs, avoiding the use of an external reducing agent.[26,27] Hence, from economic and ecological perspectives, developing a reductant- and surfactant-free method for synthesizing metal NPs is in high demand.

On the other hand, phosphines have not been explored so far for the synthesis of Ir NPs, although Ir is one of the most extensively explored precious metals, having a close, compatible relationship with phosphines in the homogeneous phase and has been involved in various path-breaking catalytic transformations.[32,33] One of the typical advantages of Ir is that ultra-small-sized nanoparticles (1–2 nm) can be synthesized by following relatively simple synthetic protocols.[34–36] It is worth mentioning that particle size is one of the most important properties of MNPs, and from a catalytic perspective, these ultra-small-sized NPs are usually more advantageous than large-sized NPs because of the higher surface-to-volume ratio. Recent literature studies suggest that ultra-small-sized MNPs, mainly with platinum group metals, can be synthesized using sterically bulky ligands (such as NHCs and phosphines) covalently attached to different supports[4,11,35] and such materials usually show enhanced catalytic activity in many important reactions, including oxidant-free alcohol dehydrogenation and nitroarene reduction.

It may be noted that transition-metal-catalyzed oxidant-free dehydrogenation of primary alcohols to acids with simultaneous hydrogen generation, commonly known as the acceptorless dehydrogenation (AD) reaction, has emerged as one of the most studied reactions in recent years.[37,38] The reaction has received significant attention not only from a synthetic chemistry perspective but also from the hydrogen economy point of view, as the evolved hydrogen can be used as an alternative energy source. Since the first report of this reaction about a decade ago,[39] a vast range of molecular catalysts, mostly with noble metals like Pd,[40,41] Ir,[42–44] Ru,[45–47] and a few non-noble metals like Co,[48] Ni,[49] Mn,[50] were developed for this transformation. However, successful heterogeneous catalysts for this reaction are extremely limited.[51–53] Thus, there is significant interest in developing efficient heterogeneous catalysts for this dehydrogenative transformation. As part of our continuing interest in the AD reaction,[52,53] herein, we demonstrate the synthesis of a silica-supported Ir nanostructured catalyst with the help of a surface-capping phosphine ligand, without the involvement of an external reducing or stabilizing agent, and explore its potential as a catalyst for dehydrogenation of primary alcohols to carboxylic acids.

To expand the scope of our catalyst (IrNPs@SiO_2), we have also investigated the catalytic activity for chemoselective hydrogenation of nitroarenes to the corresponding aminoarenes. It is worth noting that selective hydrogenation of nitroarenes is a well-established protocol for synthesizing the corresponding amines, which serve as important intermediates for the fine chemical industry.[54] However, selective reduction of nitro groups in compounds that contain other reducible functionalities like C=C, C=O, C–Cl, *etc*., often becomes challenging, as these functional groups also undergo simultaneous reduction, producing undesired products and thus influencing the selectivity.[55,56] Nevertheless, a few nanoparticle-based catalysts exist, mostly with noble metals, including Ir, that perform chemoselective reduction of nitro compounds while keeping reducible functional groups intact.[31,56–63] However, high metal loading,[59,62] high pressure,[63] limited substrate scope,[56,57] *etc*., are some of the bottlenecks that limit their industrial-scale utilization.

Experimental section

Materials

Iridium(III) chloride ($IrCl_3$, 99%) was purchased from TCI and 2-diphenylphosphinoethyl-functionalized silica gel (DPPE@SiO_2; 0.7 mmol g^{-1} loading; 200–400 US mesh) was purchased from Sigma-Aldrich. All other relevant substrates, bases and solvents were purchased from Acros Organics, Sigma-Aldrich, TCI Chemicals, SRL and RANKEM.

Material characterization

Powder X-ray diffraction (P-XRD) patterns were recorded on a Bruker AXS D8 Advance instrument over a 20–80° scanning angle (wide-angle scan) by using Cu Kα as the source. Scanning electron microscopy and energy dispersive X-ray spectrometry (SEM-EDAX) analyses were performed on a JEOL-IT300HR system. High-resolution transmission electron microscopy (HR-TEM) micrographs were acquired using a JEOL JEM-F200 microscope operating at an accelerating voltage of 200 kV, equipped with a thermal electron field-emission gun of ZrO/W. X-ray photoelectron spectroscopy (XPS) data were collected using a PHI 5000 VersaProbe II, FEI Inc system. Inductively coupled plasma atomic emission spectroscopy (ICP-AES) was performed using an ARCOS Simultaneous ICP spectrometer across the wavelength range of

130–770 nm, using an RF generator (1.6 kW, 27.12 MH) and charge-coupled devices as detectors to determine the metal content in the material. ^{1}H and ^{13}C NMR spectra were recorded at 500 MHz and 125 MHz, respectively, on a Bruker AVANCE III HD-500 MHz spectrometer/Bruker Avance Neo 500 MHz spectrometer. Electrospray ionization-mass spectrometry (ESI-MS) spectra of the catalytic products were recorded using a Thermo Fisher Ultimate 3000/TSQ Endure instrument. Gas chromatography-mass spectrometry (GC-MS) analysis was carried out on a Thermo Scientific TRACE 1600 GC-MS system, which has a capillary column of dimensions: length 30 m, I.D. 0.25 mm, and film 0.25 μm, connected to a flame ionization detector (FID).

Synthesis of the catalyst (IrNPs@SiO_2)

In a 100 mL two-necked round-bottomed flask, 2 g of DPPE@SiO_2 was dispersed in 25 mL of absolute ethanol for 30 min, followed by 10 min of ultrasonication. To the above-dispersed mixture, 25 mL of 0.5 mmol of $IrCl_3$ solution (in ethanol) was added dropwise over 25 min and subsequently stirred for 12 h. The solid mass was filtered and washed several times with small portions of distilled water, followed by isopropanol, and dried at 80 °C for 6 h in a hot air oven. Furthermore, the dried material was calcined at 450 °C for 3 h to obtain the desired catalyst (IrNPs@SiO_2).

General procedure for acceptorless dehydrogenation of alcohols

In a typical reaction, 1 mmol of alcohol (**1**), 2 mmol of *t*-BuOK, and 20 mg (0.035 mol%) of the catalyst (IrNPs@SiO_2) in 6 mL of toluene were taken in a round-bottomed flask (100 mL). The reaction mixture was refluxed at 110 °C in a pre-heated oil bath for 4 h. After completion of the reaction, the solvent was removed under reduced pressure, affording crude potassium carboxylate salt. The purified product was obtained by following either of the isolation methods. Isolation Method A: the dried carboxylate salt was washed with ethyl acetate (10 mL) three times and dried in an oven. The dried solid mass was dissolved in deionized (30 mL) water, and the catalyst was recovered using centrifugation. Subsequently, the potassium salt solution was acidified with aqueous 1 M HCl (10 mL) and extracted using ethyl acetate (20 mL), which was dried over anhydrous Na_2SO_4 and concentrated under reduced pressure to obtain the purified carboxylic acid. Isolation Method B: the carboxylate salt was washed with ethyl acetate (10 mL) three times and dried in an oven. The solid mass was dissolved in methanol (30 mL), and the catalyst was recovered by centrifugation. Subsequently, the methanol solvent was removed under reduced pressure to obtain the pure potassium carboxylate salt, eventually characterized by ESI-MS and NMR (^{1}H and ^{13}C), as presented in the ESI (Fig. S3–S24 and S25–67,† respectively).

Volumetric estimation of molecular hydrogen in the AD reaction

The volume of hydrogen gas evolved was measured using a reverse burette water displacement experiment.[44,64] The experiment was conducted in a two-necked round-bottomed flask (100 mL), which was initially dried and set up in preheated oil at 110 °C. Subsequently, the flask was charged with benzyl alcohol (**1a**, 0.5 mmol), *t*-BuOK (1 mmol), and the catalyst (0.035 mol%) in toluene. The top of the flask was closed with a glass stopcock and the other arm was fitted to a closed burette filled and dipped in water. The reaction continued until the evolution of hydrogen ceased. This experiment was conducted three times until a consistent reading was obtained. Eventually, the number of moles of hydrogen that evolved was calculated by applying the ideal gas law. The volume of the water displaced in the burette was 22.5 mL, the vapour pressure of water at 293 K was 17.5424 Torr, R = 62.3635 L Torr K^{-1} mol^{-1}, and the atmospheric pressure was 761.3126 Torr. Therefore, moles of hydrogen were calculated as $n(H_2) = [(P_{atm} - P_{water})\,V]/RT$ = 0.00092 mol (expected value: 0.001 mol).

In situ hydrogenation experiment

In a typical experiment, 1 mmol of benzyl alcohol (**1a**), 2 mmol of *t*-BuOK, (0.035 mol%) catalyst, 1 mmol of styrene, 5% Pd/C, and 6 mL of toluene were taken in a 100 mL two-necked round-bottomed flask without using any external hydrogen source. The reaction mixture was placed in a preheated oil bath at 110 °C. The reaction mixture was refluxed for 6 h, which was monitored using GC-MS.

Procedure for gram-scale synthesis of benzoic acid

The gram-scale synthesis of benzoic acid was performed in a 100 mL round-bottomed flask, which was charged with 10 mmol of benzyl alcohol (**1a**) and 25 mmol of *t*-BuOK dissolved in 20 mL of toluene, with a catalyst loading of 0.035 mol%, and placed in a pre-heated oil bath at 110 °C. The reaction was conducted for 72 h, and after completion of the reaction, benzoic acid (**2a**) was obtained by following similar procedures to those used for the general catalytic reaction.

General procedure for hydrogenation of nitroarenes

The hydrogenation reactions of nitroarenes (**3**) to the corresponding aminoarenes (**4**) were carried out by charging 1 mmol of nitroarene (**3**) and 5 mL of toluene in a stainless-steel autoclave (Parr 4838 reactor controller) made of Hastelloy, and it was initially purged with 1.1 MPa of hydrogen gas for 10 minutes, followed by the addition of 15 mg (0.026 mol%) of catalyst, IrNPs@SiO_2. The reaction temperature was set to 50 °C, and the pressure was maintained at 1.1 MPa, while stirring at 250 rpm for 5 h. Then, the reactor was cooled to room temperature and depressurized to obtain the crude reaction mixture. The progress of the reaction was monitored using TLC under UV light. Subsequently, the reaction mixture was extracted using 20 mL of ethyl acetate following the standard workup procedure, and the catalyst was recovered by centrifugation. The obtained product was purified by column chromatography over silica gel (60–120 mesh) using a hexane–ethyl acetate mixture (8 : 2), and the product was characterized by ESI-MS and NMR (^{1}H and ^{13}C) and the results are presented in the ESI (Fig. S68–S80 and S81–S108,† respectively). The same

procedure was followed for the other derivatives of nitrobenzene.

Reusability experiment

The reusability of the as-synthesized catalyst was evaluated for both the AD reaction of benzyl alcohol (**1a**) and hydrogenation of nitrobenzene (**3a**). For the AD reaction, a 100 mL round-bottomed flask was charged with benzyl alcohol (**1a**, 1 mmol), *t*-BuOK (2 mmol), IrNPs@SiO_2 [20 g (0.035 mol%)], and toluene (6 mL) and allowed to stir at 110 °C for 4 h. Upon completion of the reaction, the catalyst was separated by centrifugation and further washed with water and isopropanol several times, followed by drying. The recovered catalyst was then used again for subsequent reactions.

On the other hand, for hydrogenation, the autoclave was charged with nitrobenzene (**3a**, 1 mmol) and the IrNPs@SiO_2 catalyst [15 g (0.026 mol%)] in toluene (5 mL). The reaction was conducted under a hydrogen pressure of 1.1 MPa at 50 °C for 5 h. The catalyst was separated by centrifugation after completion of the reaction, washed several times with water, followed by isopropanol, and dried. The subsequent reactions were performed with the recovered catalyst, maintaining the same stoichiometric ratios.

Heterogeneity test

To examine any leaching of the active metal species from the catalyst, a hot filtration test was performed. Initially, the test was conducted by reacting benzyl alcohol (**1a**, 1 mmol) and *t*-BuOK (2 mmol) in the presence of IrNPs@SiO_2 [20 mg (0.035 mol%)] in toluene (6 mL). The reaction mixture was refluxed at 110 °C, and the reaction time was shortened from 4 h to a period of 1 h. The carboxylate salt and the catalyst were filtered off from the reaction mixture under hot conditions. The resulting filtrate was further allowed to react for another 3 h under refluxing conditions at 110 °C.

In a similar experiment, nitrobenzene (**3a**, 1 mmol) was allowed to react at 50 °C under a pressure of 1.1 MPa H_2 in the presence of 15 mg (0.026 mol%) of IrNPs@SiO_2 in an autoclave. The reaction time was shortened from 5 h to a period of 1 h. Subsequently, the catalyst was filtered off from the reaction mixture under hot conditions, and the resulting filtrate was allowed to react under the same conditions for another 4 h.

Results and discussion

Synthesis and characterization

The silica-supported nanostructured Ir catalyst (IrNPs@SiO_2) was synthesized *via* a one-step wet chemical approach (Scheme 1) by reacting $IrCl_3$ with commercially available phosphine-functionalized silica gel, following a reported procedure used for the preparation of conceptually similar Pd nanoparticles.[28]

To understand the morphology and structural features of the nanomaterials, HR-TEM, SEM-EDAX, XRD, and XPS analyses were performed. The transmission electron microscopy (TEM) images obtained for IrNPs@SiO_2 at different magnifications showed the formation of nearly spherical and monodisperse nanostructured Ir particles, which were evenly distributed over the silica support (Fig. 1a–c). The particle size distribution histogram depicts ultrasmall and uniform-sized Ir particles with a size of 1.8 ± 0.5 nm (Fig. 1a inset). The HR-TEM images of IrNPs@SiO_2 revealed the presence of two different

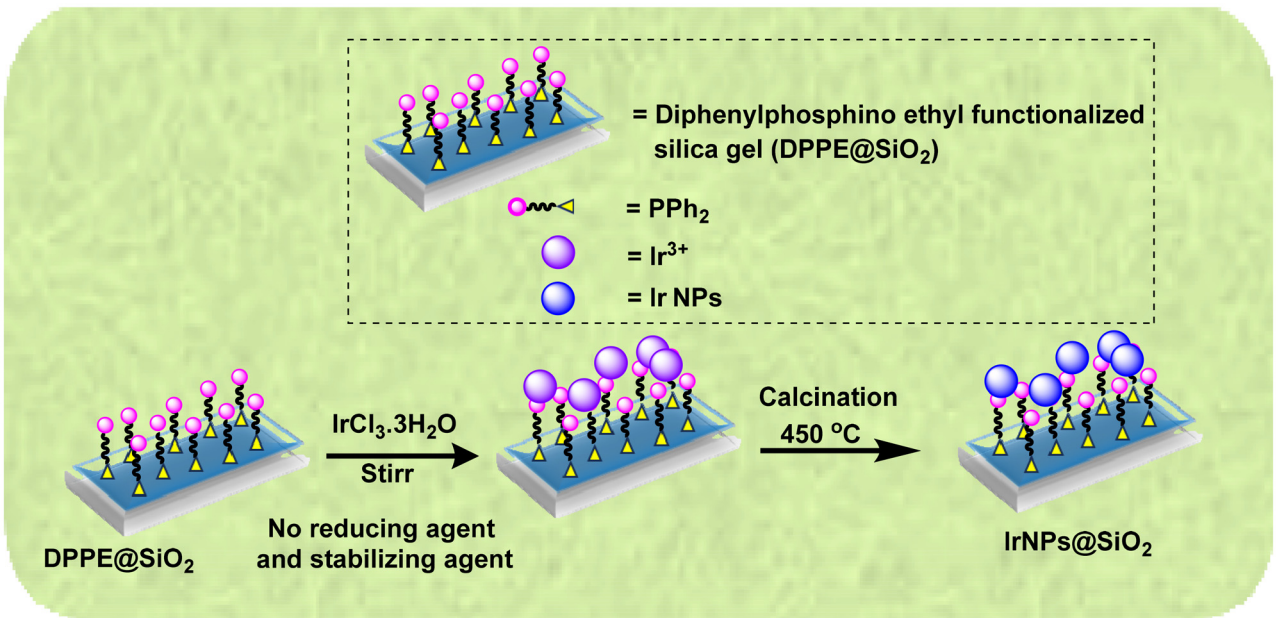

Scheme 1 Schematic representation for the synthesis of the silica-supported Ir nanostructured catalyst using the incipient wet-impregnation method.

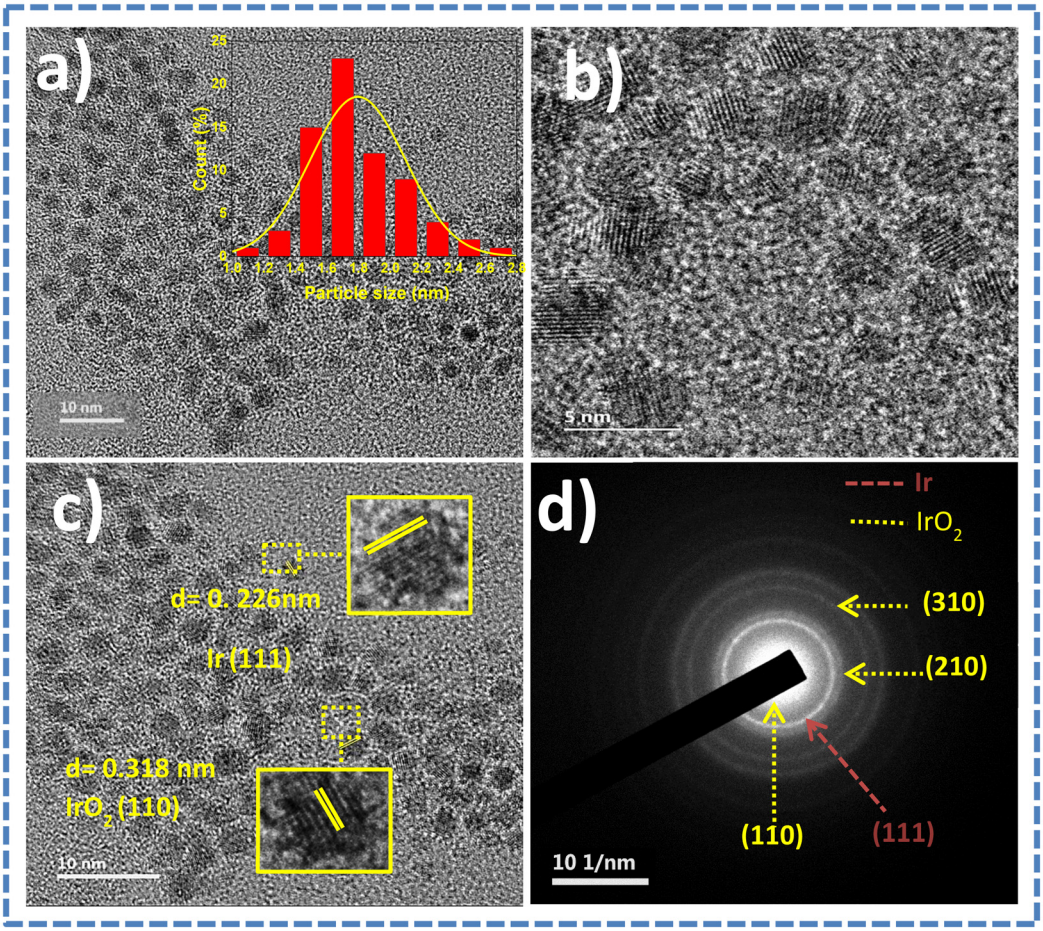

Fig. 1 (a) TEM micrographs, along with the particle size distribution histogram as the inset, (b) HR-TEM micrographs, (c) HR-TEM micrographs (showing lattice fringes along with the *d*-spacing values) of IrNPs@SiO_2, and (d) SAED diffraction pattern of IrNPs@SiO_2.

lattice spacings of 0.226 nm and 0.318 nm that correspond to Ir(111) and IrO_2(110) planes, respectively. The SAED pattern of IrNPs@SiO_2 demonstrates continuous rings corresponding to the various planes of metallic Ir and IrO_2 phases (Fig. 1d). The scanning electron microscopy (SEM) analysis depicted a morphology of silica particles with irregular shapes with sharp ridges, closely resembling with the SEM images reported for silica-supported nanoparticles (Fig. S1a and S1b†).[28,65] The presence of Ir phases was further confirmed by EDAX analysis performed over a selected area (Fig. S1c†). The powder X-ray diffraction (P-XRD) patterns of IrNPs@SiO_2 showed reflections at 40.52°, 47.3°, and 68.6° (Fig. 2), corresponding to the lattice planes of (111), (200), and (220), respectively, for face-centered cubic metallic Ir.[66] Also, some reflections were observed at 28.3°, 35.7°, 57.4°, and 64.6°, corresponding to the lattice planes of (101), (110), (220), and (310), respectively, for the rutile phase of the tetragonal crystal structure of IrO_2 (Fig. 2).[36,67–69] In addition, a broad peak at around 22.48° was observed due to the (111) plane of silica, and this value is very much similar to the corresponding plane for phosphine-functionalized silica gel (2θ = 22.403°),[28] suggesting that silica maintains its mesoporosity even after Ir loading. X-ray photoelectron spectroscopy (XPS) was performed to understand the

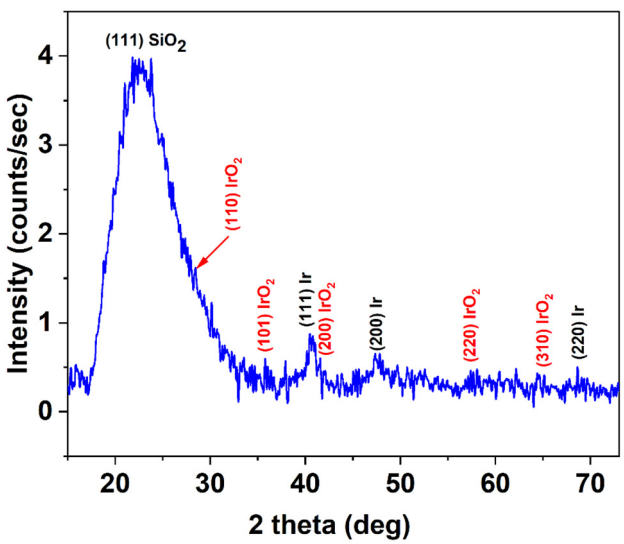

Fig. 2 Wide-angle powder X-ray diffraction pattern of IrNPs@SiO_2.

elemental composition and chemical state of Ir in IrNPs@SiO_2 (Fig. 3a). The deconvolution of the high-resolution spectra for Ir in the 4f region exhibited four discernible binding energy

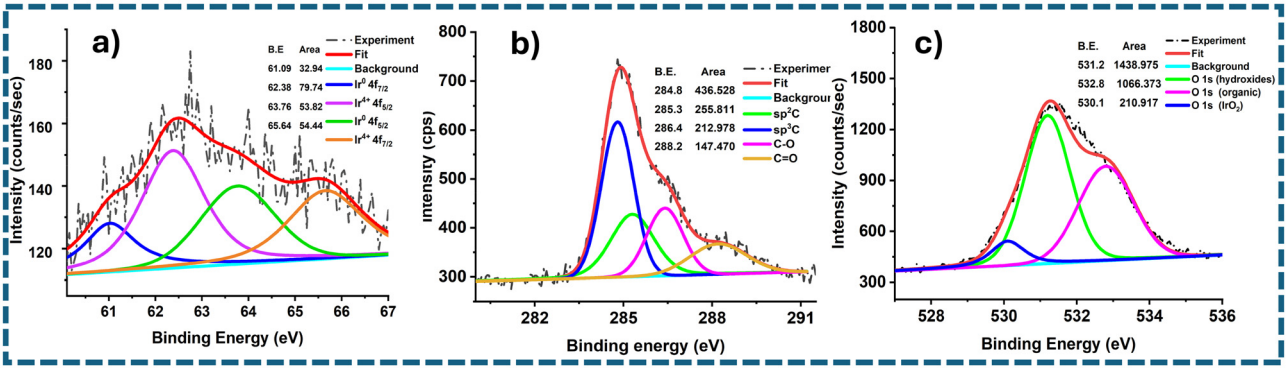

Fig. 3 Representative XPS spectra of (a) iridium, (b) carbon, and (c) oxygen in IrNPs@SiO_2 (B.E = binding energy).

peaks at 61.08, 62.34, 63.17, and 65.67 eV. Among them, the peaks at 61.08 and 63.17 eV are attributed to Ir $4f_{7/2}$ and Ir $4f_{5/2}$ states, respectively, coherent with the values for Ir(0) species. The other two peaks at 62.34 and 65.67 eV could be assigned to Ir $4f_{5/2}$ and Ir $4f_{7/2}$ electronic states, coherent with the values for Ir in the +4 state.[69,70] It is important to note that there are literature precedents available where the formation of the Ir metallic state is often accompanied by an IrO_2 state, which is due to the oxidation of the outer shell of the material under thermal conditions.[71] The deconvoluted high-resolution C_{1s} spectrum (Fig. 3b) shows four distinct peaks at 284.8 eV, 285.3 eV, 286.4 eV, and 288.2 eV, corresponding to sp^2 hybridized carbon (C=C), sp^3 hybridized carbon (C–H or C–C), C–O and C=O bonds, respectively.[72] In the O_{1s} region, a peak appears at 530.1 eV, attributable to the oxygen atom of iridium oxide (IrO_2).[73] In addition, two other peaks are observed at 531.2 and 532.8 eV, which correspond to oxygen atoms of SiO_2 and the hydroxyl groups present on the silica surface.[73,74]

The amount of Ir present in the synthesized material, IrNPs@SiO_2, was detected by ICP-AES analysis and found to be 0.33 wt%.

Catalytic study for acceptorless dehydrogenation of alcohols

The nanostructured material, IrNPs@SiO_2, was tested for the AD reaction of primary alcohols to produce carboxylic acids and molecular hydrogen. The initial optimization study was performed in toluene using benzyl alcohol (**1a**, 1 mmol) as the model substrate in the presence of 0.035 mol% (20 mg) catalyst and 1 mmol of *t*-BuOK as the base. We are gratified to see that, after a period of 12 h, almost a quantitative amount of potassium benzoate was formed, which upon treatment with 1 M HCl converted to benzoic acid (**2a**) with 74% yield (Table S1,† entry 1). As stated earlier, the AD reaction of alcohols to acids is accompanied by two equivalents of molecular hydrogen as the byproduct. To verify the evolution of hydrogen, an *in situ* styrene hydrogenation experiment was conducted using 5% Pd/C as a catalyst without any external hydrogen source. After a reaction time of 6 h, ethylbenzene was obtained in 60% yield, demonstrating that the evolved gas from the AD reaction is hydrogen. To further validate the fact that two equivalents of molecular hydrogen evolved during the reaction process, a standard reverse burette water displacement experiment was performed. The volume of the water displaced was 22.5 mL, which corresponds to 0.92 mmol of molecular hydrogen, thus confirming the evolution of two equivalents of hydrogen. Subsequently, a series of optimization studies were performed using benzyl alcohol (**1a**), with different solvents (isopropanol, water, hexane, THF, and acetonitrile), bases (*t*-BuOK, *t*-BuONa, KOH, NaOH, and Cs_2CO_3), temperatures, and catalyst loadings to achieve the most suitable conditions (*t*-BuOK, toluene, 0.035 mol% catalyst, and 110 °C), where benzoic acid (**2a**) was obtained in good yield (85%) with a TON of 2429 and a TOF of 607 h^{-1} (Table S1,† entry 2; Table 1, entry 1). It was observed that the activity dropped when toluene was replaced with other solvents (isopropanol, water, hexane, THF, and acetonitrile). It is interesting to note that the AD reaction can be scaled up, and in the gram-scale experiment, benzyl alcohol (**1a**) afforded 76% yield of benzoic acid (**2a**) with a TON of 2171.

Using the optimized conditions, we evaluated the scope of our catalyst with a variety of benzyl alcohols containing different electron-donating and electron-withdrawing substituents. Benzyl alcohols bearing electron-withdrawing groups like –Cl and electron-donating groups such as $–OCH_3$, $–CH_3$, and *-tert*-butyl produced excellent yields of the corresponding *para*- and *meta*-substituted acid products. For instance, *p*-chlorobenzyl alcohol and *p*-methylbenzyl alcohol were converted to their corresponding acids with remarkable yields of 92% and 97% (Table 1, entries 2 and 7, respectively). However, the *ortho*-substituted benzyl alcohols furnished relatively lower yields compared to *meta*- and *para*-substituents, which might be attributed to steric crowding. For example, *o*-methylbenzyl alcohol produced only 51% of the corresponding acid, while *p*-methylbenzyl alcohol yielded 97% (Table 1, entries 5 and 7, respectively). Interestingly, despite the presence of electron-withdrawing halogen substituents at the *ortho* position, *o*-chlorobenzyl alcohol was converted to *o*-chlorobenzoic acid with a yield of 94% (Table 1, entry 4). Similar results were obtained with the *o*-bromo substrate, which afforded an 80% yield (Table 1, entry 13). It is noteworthy that in some cases, prolonged reaction times led to the dehalogenation of benzyl alcohols.[75]

Table 1 Acceptorless dehydrogenation of various primary alcohols to their corresponding carboxylates using IrNPs@SiO_2 as the catalyst[a]

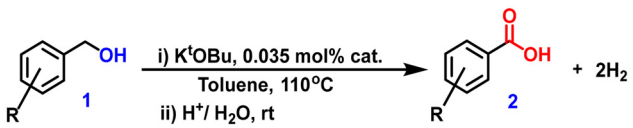

Entry	Substrate	Product	Time (h)	Yield[b] (%)	TON
1	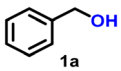 1a	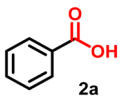 2a	4	85	2429
2	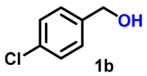 1b	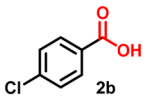 2b	6	92	2629
3	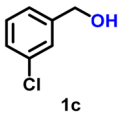 1c	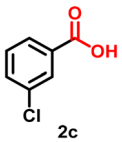 2c	6	89	2543
4	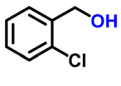 1d	 2d	10	94	2686
5	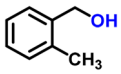 1e	 2e	10	51	1457
6	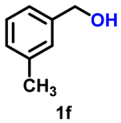 1f	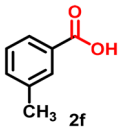 2f	6	86	2457
7	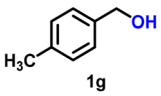 1g	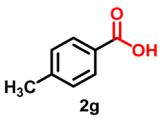 2g	6	97	2771
8	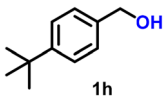 1h	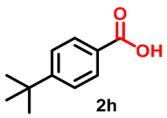 2h	10	91	2600
9	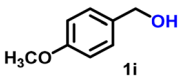 1i	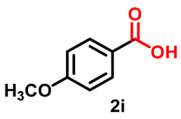 2i	6	92	2628
10	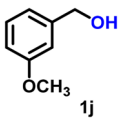 1j	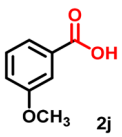 2j	6	95	2714
11	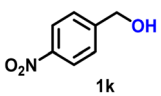 1k	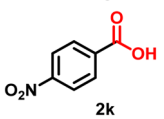 2k	10	55	1571
12	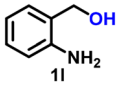 1l	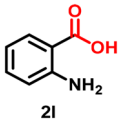 2l	10	72	2057

Table 1 *(Contd.)*

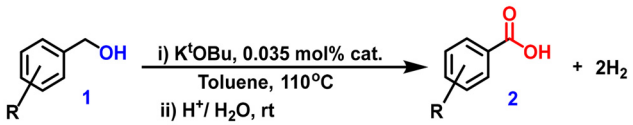

Entry	Substrate	Product	Time (h)	Yield[b] (%)	TON
13	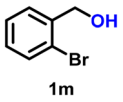 1m	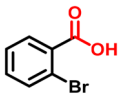 2m	10	80	2286
14	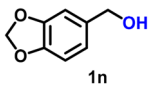 1n	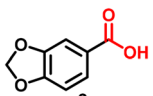 2n	10	88	2514
15	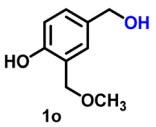 1o	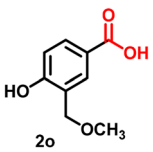 2o	18	94	2686
16	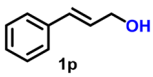 1p	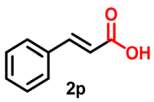 2p	10	65	1857
17	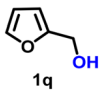 1q	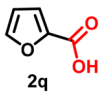 2q	10	45	1286
18	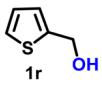 1r	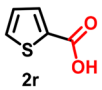 2r	10	80	2286
19	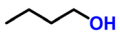 1s	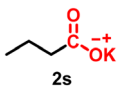 2s	18	60	1714
20	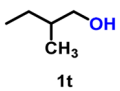 1t	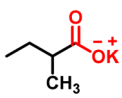 2t	18	55	1571
21	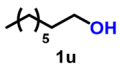 1u	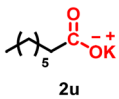 2u	18	54	1543
22	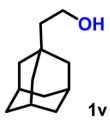 1v	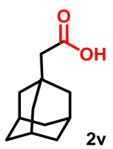 2v	18	55	1571

[a] All the reactions were carried out using 1 mmol of substrate (**1**), 0.035 mol% catalyst, and 2 mmol of *t*-BuOK in 6 mL of toluene at 110 °C. [b] Isolated yields are reported in parentheses.

Interestingly, with our catalyst, no dehalogenation was observed, and the selectivity for the desired product was maintained. Moreover, nitro-substituted benzyl alcohols typically show poor results and are often accompanied by their amino analogues.[76] In our system, a nitro group at the *para* position resulted in a 55% yield of *p*-nitrobenzoic acid (Table 1, entry 11). After a comprehensive evaluation of benzyl alcohol derivatives with our catalyst, we successfully applied the reaction protocol to a handful of biomass-derived alcohols, including piperonyl alcohol, vanillyl alcohol, furfuryl alcohol, and thiophene ethanol, achieving good to excellent yields of their corresponding acids (Table 1, entries 14, 15, 17 and 18). It may be noted that in recent years, the utilization of biomass-based substrates for different types of hydrogen evolution reactions has gained tremendous significance from the hydrogen economy point of view.[77–80] Moreover, the acids obtained from

biomass-derived alcohols have a wide range of applications in medicine and the chemical industry; for example, piperonylic acid is used as an anticancer, anti-inflammatory, and antioxidant agent.[81,82] Additionally, our catalyst can convert aliphatic alcohols, typically difficult to activate, into their corresponding carboxylic acids. For instance, octan-1-ol and adamantane-ethanol were converted to their respective acids with yields of 54% and 55% (Table 1, entries 21 and 22).

As mentioned earlier, there are several homogeneous catalysts reported for this transformation; however, only a limited number of successful heterogeneous catalysts are known to date. Hence, in order to understand the current state of our catalytic system, a detailed literature survey on the heterogeneous-catalysed AD reaction of alcohols to acids has been performed and is presented in Table 2. Although, in terms of yields, our catalyst shows comparable results with some of the reported heterogeneous catalysts, in terms of catalyst loading and substrate scope, our catalyst is much superior to the existing ones.

Plausible mechanism

Based on literature precedents, a plausible mechanism has been proposed for the AD reaction of primary alcohols to carboxylic acids (Scheme 2).[53] It is very likely that, at the initial stage, the alcohol molecule is adsorbed onto the catalyst surface, forming species **I**, which upon rearrangement produces an alkoxide-based intermediate **II**, followed by β-hydride elimination to form the metal-hydride intermediate **III**. Then, one molecule of H_2 gas is released from intermediate **III** to produce an aldehyde-based intermediate **IV**, which undergoes a nucleophilic attack by the K^{t}OBu base at the aldehyde site, generating intermediate **V**. Treatment of a second molecule of K^{t}OBu with intermediate **V** produces the potassium carboxylate-based intermediate **VI** with concomitant generation of

Table 2 Comparison of various reported noble metal-based systems for the acceptorless dehydrogenation of alcohols to carboxylic acids

Catalyst	Conditions	Substrate scope	Yields	Reference
Ir@NiO	0.15 mol%, 6 h, KOH, toluene, 110 °C	Benzyl alcohols, aliphatic alcohols, biomass-derived heterocyclic alcohols	17–98%	Bordoloi *et al.* (2023)[53]
Pd@NiO	0.08 mol%, 6 h, KOH, toluene, 110 °C	Benzyl alcohols, aliphatic alcohols, biomass-derived heterocyclic alcohols	22–97%	Bordoloi *et al.* (2022)[52]
Ru@Co-NC	2–8 wt%, 24 h, toluene, 120 °C	Benzyl alcohols, aliphatic alcohols	20–83%	Chen *et al.* (2023)[83]
MnFe–S–Ag	14.5 wt%, 24 h, mesitylene, 160 °C	Benzyl alcohols, aliphatic alcohols	60–92%	Yazdani *et al.* (2020)[75]
Rh/C	20 mol%, NaOH, H_2O, 100 °C, 6 h	Benzyl alcohols, one aliphatic alcohol (decanol)	29–89%	Sawama *et al.* (2014)[84]
Pd/C	5 mol%, NaOH, H_2O, 80 °C, 6 h, 800 hPa	Benzyl alcohols, one aliphatic alcohol (decanol)	55–100%	Sawama *et al.* (2015)[51]
Ir@PPh$_2$SiO$_2$	0.035 mol%, 4 h, K^{t}OBu, toluene, 110 °C	Benzyl alcohols, aliphatic alcohols, biomass-derived heterocyclic alcohols	40–95%	This work

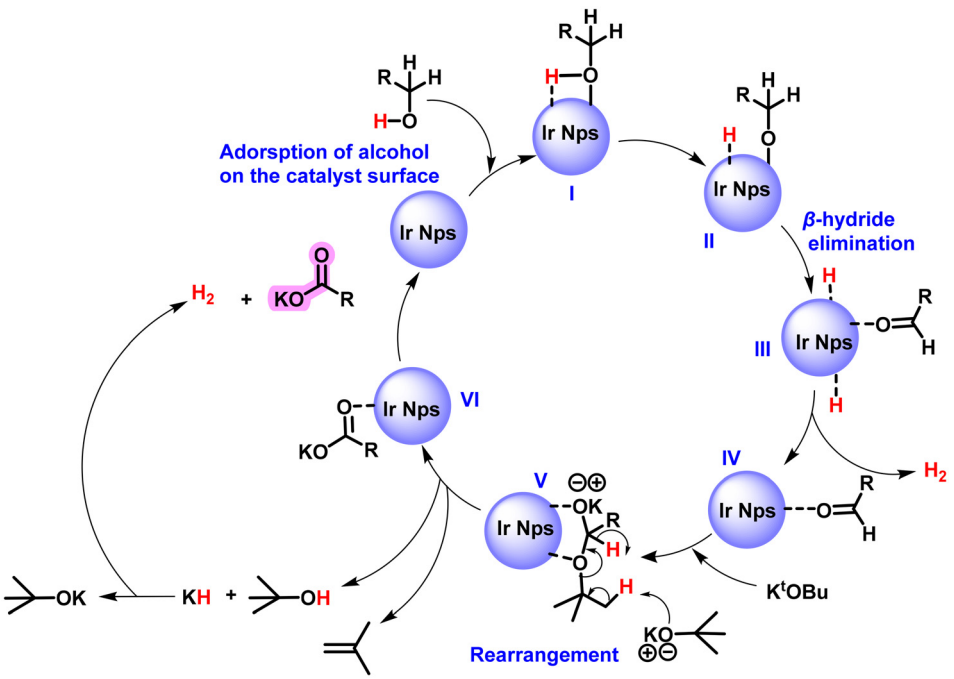

Scheme 2 Plausible mechanism for carboxylic formation from a primary alcohol using IrNPs@SiO_2 as the catalyst.

Table 3 Chemoselective hydrogenation of various nitrobenzenes to their corresponding aminobenzenes using IrNPs@SiO_2 as the catalyst[a]

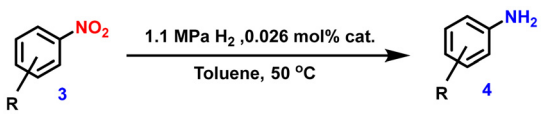

Entry	Substrate	Product	Yield[b] (%)	TON
1	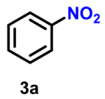 3a	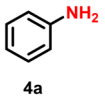 4a	58	2231
2	 3b	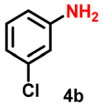 4b	70	2692
3	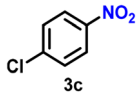 3c	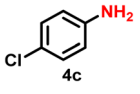 4c	56	2154
4	 3d	 4d	59	2269
5	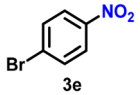 3e	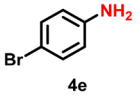 4e	61	2346
6	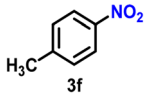 3f	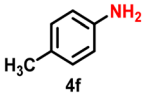 4f	92	3538
8	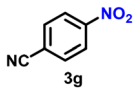 3g	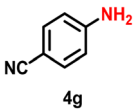 4g	76	2923
9	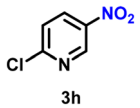 3h	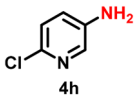 4h	73	2808
10	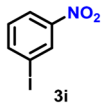 3i	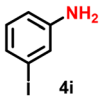 4i	56	2154
11	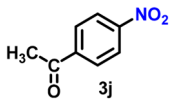 3j	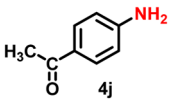 4j	93	3577
12	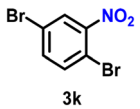 3k	 4k	50	1923
13	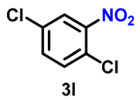 3l	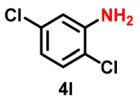 4l	56	2154
14	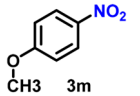 3m	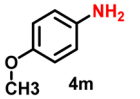 4m	78	3000

Table 3 *(Contd.)*

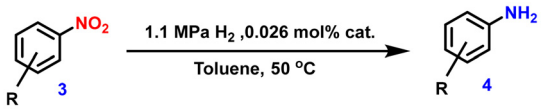

Entry	Substrate	Product	Yield[b] (%)	TON
15	 3n	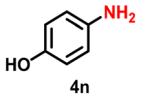 4n	53	2028

[a] All the reactions were carried out using 1 mmol of substrate (**3**), 0.026 mol% catalyst, and 1.1 MPa H_2 pressure in 5 mL of toluene for a reaction time of 5 h. [b] Isolated yields are reported in parentheses.

hydrogen and a highly volatile isobutene molecule. It may be noted that this type of isobutene formation pathway for the oxidation of aldehydes to carboxylic acids in the presence of K^tOBu as the base was proposed by Rashid's group in recent work.[85] On desorption of the carboxylate group from intermediate **VI**, potassium carboxylate is formed, which upon acidic workup produces the required carboxylic acid.

Catalytic study for hydrogenation of nitroarenes

As Ir-based nanomaterials are well known for showing good catalytic activity towards hydrogenation reactions, we have also explored the activity of our nanostructured Ir catalyst for chemoselective hydrogenation of various nitroarenes to aminoarenes. This reaction has considerable importance in the pharmaceutical and fine chemical industries, as many intermediate amines can be easily synthesized through this method. Although there are a large number of reports on the catalytic reduction of nitroarenes to aminoarenes with noble-metal-based heterogeneous catalysts, there are only very few reports on Ir-based heterogeneous catalysts for this transformation.[36,56,61] In the initial optimization study, nitrobenzene (**3a**) was used as the substrate and ethanol as the solvent, as this condition produced the best results for other catalytic processes.[11] Initially, the reaction was conducted in ethanol, but a solvent optimization study indicated that toluene is the most effective solvent for the hydrogenation of nitrobenzene with our catalyst, resulting in a yield of 58% after 5 h (Table S2,† entry 1; Table 3, entry 1). It was observed that hydrogen pressure plays a significant role in the reaction dynamics. Varying the pressure from 1.1 MPa to 0.5 MPa resulted in minimal product conversion (Table S2,† entry 7). Similarly, other parameters such as temperature and catalyst loading were varied to obtain the optimal conditions for the reaction. The best results were achieved with a catalyst loading of 0.026 mol%, a hydrogen pressure of 1.1 MPa, and a reaction time of 5 h in toluene (Table S2,† entry 1). Under these optimized conditions, we examined the scope of our catalyst for a range of nitroarenes containing electron-donating and electron-withdrawing groups, and remarkably good yields were obtained, and the results are summarized in Table 3. Our

results indicated that nitroarenes containing electron-donating groups, such as $-CH_3$ and $-OCH_3$, at the *para* position, produced good yields of the product, achieving 92% and 78%, respectively (Table 3, entries 6 and 14). In contrast, the presence of electron-withdrawing groups, such as –Cl, –Br, and –I, resulted in relatively lower yields, regardless of their positioning at the *para* or *meta* positions. It is important to note that haloanilines, *viz.*, chloroaniline (CAN), are significant agrochemical amines;[86] however, their production often involves dechlorination, leading to the formation of aniline as a side product.[87,88] In our study, despite obtaining a lower yield of *para*-chloroaniline in about 56%, we did not encounter any dechlorination (Table 3, entry 3). Additionally, our catalyst successfully produced 2,5-dibromoaniline (50%) and 2,5-dichloroaniline (56%) from their corresponding nitro substrates, with their halogen groups retained (Table 3, entries 12 and 13, respectively). Furthermore, *p*-nitrophenol (PNP) is a hazardous environmental pollutant[36,89,90] that can be effectively reduced by our catalyst to *p*-aminophenol, yielding a moderate conversion of 53% (Table 3, entry 15). Notably, even in the presence of the electron-withdrawing *p*-$COCH_3$ group, we achieved an excellent product yield of 93% (Table 3, entry 11). We observed that steric factors significantly influenced the reactivity of *ortho*-substrates. For example, a considerably lower conversion was obtained for *o*-chloronitrobenzene. Similarly, heteroaromatic substrates like 2-chloro-5-nitropyridine produced the pharmaceutically important 2-chloro-5-aminopyridine with a moderate yield of 73% (Table 3, entry 9).

It may be noted that although several platinum group metal-based heterogeneous catalysts have been reported for the hydrogenation of nitroarenes, only a handful of Ir-based catalysts are known to date. In order to understand the current state of our catalytic system, we performed a detailed literature survey on heterogeneous catalysed nitro-aromatic reduction

Table 4 Comparison of various reported noble metal-based systems for the hydrogenation of nitrobenzene to aminobenzene under liquid phase conditions

Catalyst	Conditions	Substrate scope	Yields	Reference
Ir@H102-350	0.17 mol%, 30 min, 1.5 MPa, RT, methanol	*p*,*o*,*m*-Substituted nitrobenzenes	100%[b]	Zhang *et al.* (2021)[62]
IrFe	10 wt%, 1.7 h, 0.3 MPa, 40 °C, toluene	*m*-Nitrostyrene	99%[b]	Lu *et al.* (2016)[56]
Pd@MoS_2	3 wt%, 1.5 h, 4 MPa, 80 °C	*p*,*o*,*m*-Substituted nitrobenzenes	96–100%[b]	Zhu *et al.* (2024)[32]
Pd-DPPE@SiO_2	0.84 wt%, 30 min, 1 MPa, 50 °C, ethanol	*p*,*o*,*m*-Substituted nitrobenzenes	83–100%[b]	Kalita *et al.* (2019)[11]
Pd@NAC-800	0.5 mol%, 2 h, 0.1 MPa, ethanol	*p*,*o*,*m*-Substituted nitrobenzenes	96–100%[b]	Li *et al.* (2014)[31]
Pd/Al_2O_3	0.35 wt%, 1.1 MPa, 100 °C	*p*-Chloronitrobenzene	100%[b]	Wang *et al.* (2012)[91]
Pd/ZnO	4.7 wt%, 3 h, 0.1 MPa, 180 °C,	*p*-Chloronitrobenzene	92%[b]	Lizana *et al.* (2013)[57]
Ir@PPh_2SiO_2	0.026 mol%, 5 h, 1.1 MPa, 50 °C toluene	*p*,*o*,*m*-Substituted nitrobenzenes	41–85%[a]	Present work

[a] Isolated yields. [b] Determined by GC analysis.

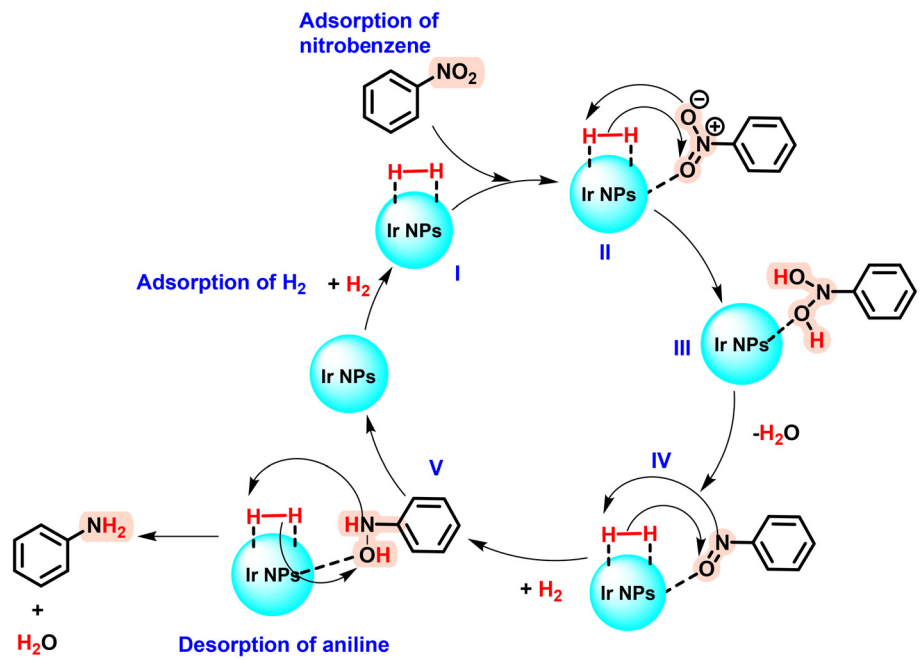

Scheme 3 Plausible mechanism for aminoarene formation from nitroarenes using IrNPs@SiO_2 as the catalyst.

reactions, and the results are presented in Table 4. Usually, our catalyst exhibits relatively lower yields compared to some of the reported Ir-[62] or Pd-based[32] catalysts. However, in terms of catalyst loading and substrate scope, the present catalyst seems much superior compared to the reported ones.

Plausible mechanism

Based on literature evidence, a plausible mechanism for the hydrogenation of nitroarenes to aminoarenes has been proposed and is displayed in Scheme 3.[92] Initially, the hydrogen and the nitrobenzene molecule are adsorbed onto the surface of the catalyst, forming species **I** and **II**, respectively. The nitro-based species **II** is protonated to form intermediate **III**, which releases one molecule of H_2O to form a nitroso-based intermediate **IV**. This nitroso-based intermediate **IV** is protonated to form a hydroxylamine intermediate **V**, followed by abstraction of protons to form an aniline molecule, which is desorbed from the catalyst surface.

We conducted a hot filtration experiment to evaluate the heterogeneity of our catalyst for the two reactions: the AD reaction of benzyl alcohols and the hydrogenation of nitroarenes. Our results indicated that, in both cases, there was no evidence of Ir metal leaching into the reaction solution. Therefore, we confirm that our catalyst is heterogeneous in nature (Fig. 4a and b).

Reusability experiments were conducted using model substrates for both the AD reaction and nitroarene hydrogenation. Our results indicate that the catalyst can be reused for up to five consecutive cycles without a significant loss in activity (Fig. 4c and d); however, from the sixth cycle onwards, some gradual loss in activity has been noticed. To investigate the characteristics of the recycled catalyst, we performed P-XRD (Fig. S2†), HR-TEM (Fig. 5), and SEM-EDX (Fig. S1d, S1e, and S1f†) analyses for the catalyst after the fifth cycle of nitrobenzene hydrogenation. The TEM micrograph of the reused catalyst shows uniformly sized nanoparticles that are evenly distributed and exhibit no signs of agglomeration, similar to the fresh catalyst. This indicates that our catalyst remains stable even after multiple uses. Additionally, the SEM-EDX and P-XRD analyses of the catalyst used up to five times reveal a

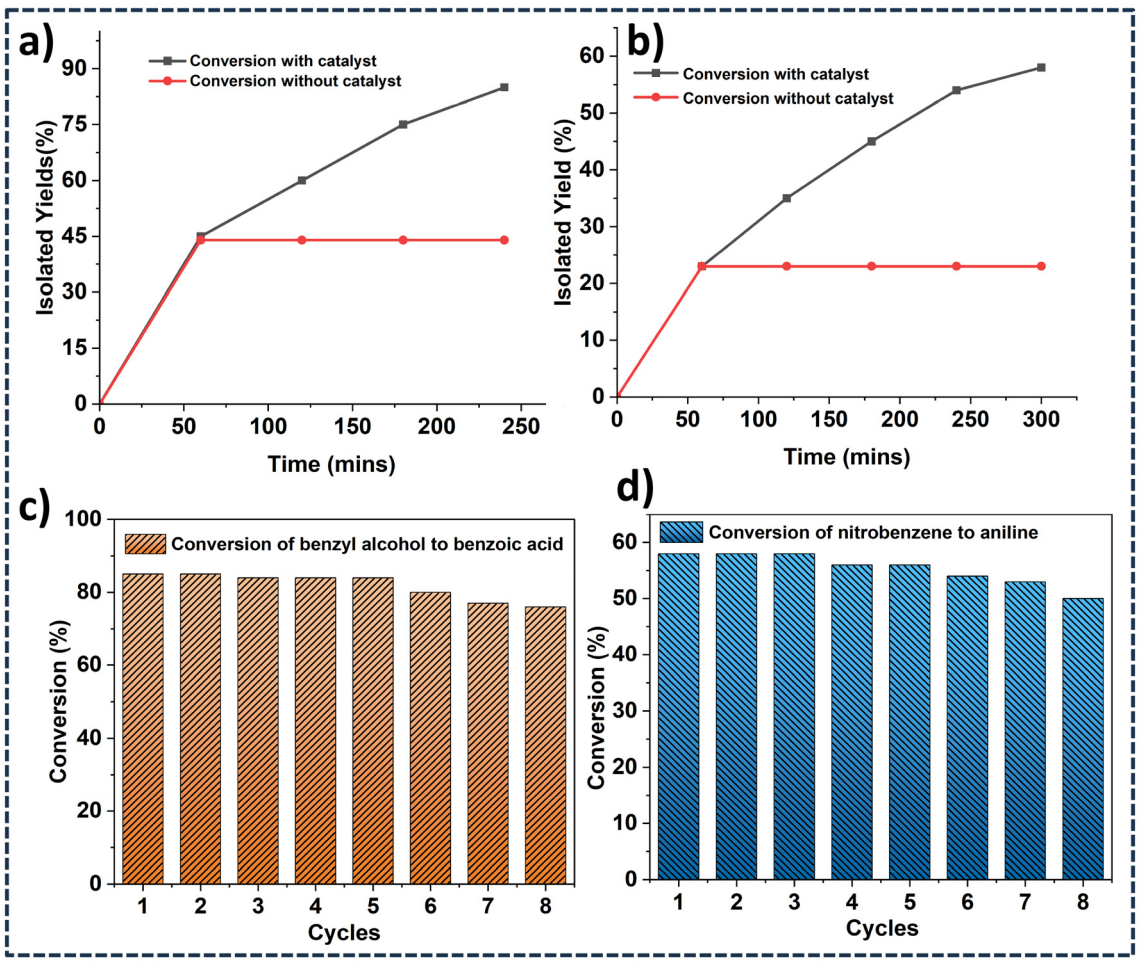

Fig. 4 Heterogeneity test for (a) the acceptorless dehydrogenation reaction of benzyl alcohol and (b) hydrogenation of nitrobenzene; plots of conversion *versus* catalytic cycles for the recyclability of the catalyst IrNPs@SiO_2 up to the fifth cycle for (c) benzyl alcohol to benzoic acid and (d) nitrobenzene to aniline.

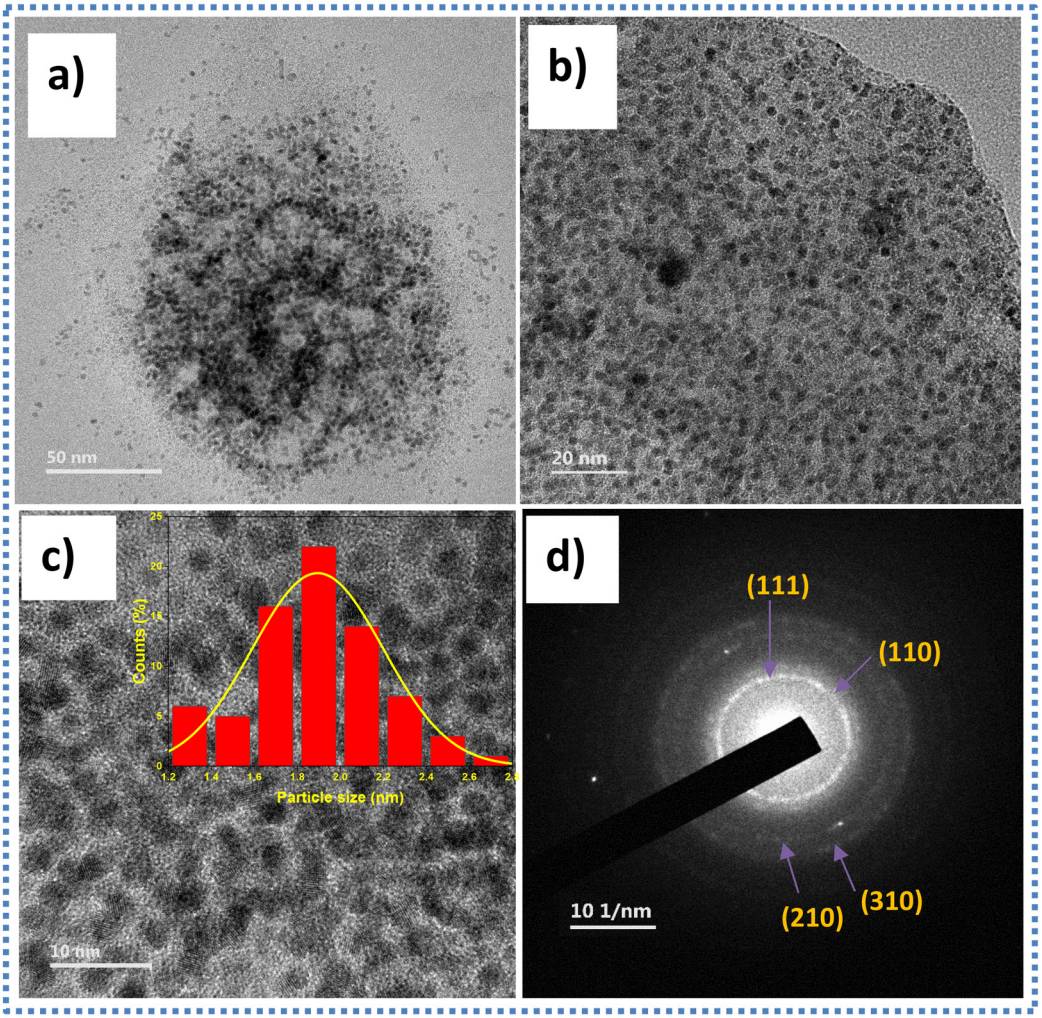

Fig. 5 (a) and (b) TEM micrographs, (c) HR-TEM image with the corresponding size distribution (inset), and (d) SAED pattern of the recycled catalyst up to the fifth run for hydrogenation of nitrobenzene.

similar morphology and structure, sustaining the respective planes for Ir, as observed in the fresh sample. This suggests that our catalyst has the potential for even more catalytic runs.

Conclusion

In summary, we developed a phosphine-ligand-induced nanostructured Ir catalyst supported on silica, capable of acting as a recyclable catalyst for two important reactions *viz*. acceptorless dehydrogenation of primary alcohols to carboxylic acids with concomitant generation of molecular hydrogen and chemoselective hydrogenation of nitroarenes to aminoarenes. The catalyst synthesis is a straightforward one-step process that involves the reaction of $IrCl_3$ with commercially available phosphine-functionalized silica gel *via* a wet chemical approach. Notably, this is the first example of a ligand-based synthesis of Ir NPs without involving an external reducing or stabilizing agent. In the acceptorless dehydrogenation, a wide range of alcohols, including relatively less reactive aliphatic and biomass-based alcohols, can be easily converted to their corresponding carboxylates with low catalyst loading (with a TON of up to 2771 for 4-methylbenzyl alcohol). Our catalyst's overall efficacy and substrate scope are significantly superior to those of the state-of-the-art Ir-based heterogeneous catalysts reported to date for this transformation. Like the AD reaction, a range of nitroarenes, particularly those containing other reducible functionalities such as C═N C═O, *etc*., can be selectively converted to the corresponding aminoarenes with moderate to excellent yields under mild reaction conditions. For both reactions, the catalyst was found to be recyclable for at least five consecutive runs without compromising yields.

Author contributions

Jyotishma Baruah – data collection, data analysis, data interpretation, and drafting of the article. Pankaj Das –

concept or design of the work, critical revision of the article, and final approval of the version to be published.

Data availability

The authors confirm that the data supporting the findings of this study are available within the article and in its ESI.†

Conflicts of interest

The authors have no conflicts of interest to declare.

Acknowledgements

The authors gratefully acknowledge DST- SERB, New Delhi (CRG/2022/000672), DST-PURSE (SR/PURSE/2022/143 (C)) and DST-FIST (SR/FST/CS-1/2020/152) for financial support. The authors thank CSIC Dibrugarh University, IIT Kanpur, IISER Mohali, IIT Bombay, and BITS Pilani Goa for various characterization facilities. Special thanks to Dr Gauravjyoti Dutta Kalita for his suggestions at different stages of this work.

References

1 L. H. Pignolet, *Homogeneous Catalysis with Metal Phosphine Complexes*, Springer Science Business Media. Plenum Press, New York, 2013.
2 M. L. Clarke and J. J. R. Frew, Ligand Electronic Effects in Homogeneous Catalysis Using Transition Metal Complexes of Phosphine Ligands, In *SPR Organometallic Chemistry*, ed. I. J. S. Fairlamb and J. M. Lynam, 2009, vol. 35, pp. 19–46.
3 D. González-Gálvez, P. Nolis, K. Philippot, B. Chaudret and P. W. N. M. Van Leeuwen, *ACS Catal.*, 2012, **2**, 317–321.
4 M. Ibrahim, M. M. Wei, E. Deydier, E. Manoury, R. Poli, P. Lecante and K. Philippot, *Dalton Trans.*, 2019, **48**, 6777–6786.
5 M. Ibrahim, M. A. S. Garcia, L. L. R. Vono, M. Guerrero, P. Lecante, L. M. Rossi and K. Philippot, *Dalton Trans.*, 2016, **45**, 17782–17791.
6 S. U. Son, Y. Jang, K. Y. Yoon, E. Kang and T. Hyeon, *Nano Lett.*, 2004, **4**, 1147–1151.
7 D. Poier, O. Loveday, M. E. Usteri, D. Stoian, N. López, S. Mitchell, R. Marti and J. Pérez-Ramírez, *ACS Nano*, 2025, **19**, 1424–1432.
8 N. J. S. Costa and L. M. Rossi, *Nanoscale*, 2012, **4**, 5826–5834.
9 L. M. Rossi, J. L. Fiorio, M. A. S. Garcia and C. P. Ferraz, *Dalton Trans.*, 2018, **47**, 5889–5915.
10 J. De Roo, *Chem. Mater.*, 2023, **35**, 3781–3792.
11 G. D. Kalita, P. P. Sarmah, P. K. Saikia, L. Saikia and P. Das, *New J. Chem.*, 2019, **43**, 4253–4260.
12 R. Xiao, J. Jia, R. Wang, Y. Feng and H. Chen, *Acc. Chem. Res.*, 2023, **56**, 1539–1552.
13 H. Guan, C. Harris and S. Sun, *Acc. Chem. Res.*, 2023, **56**, 1591–1601.
14 A. Heuer-Jungemann, N. Feliu, I. Bakaimi, M. Hamaly, A. Alkilany, I. Chakraborty, A. Masood, M. F. Casula, A. Kostopoulou, E. Oh, K. Susumu, M. H. Stewart, I. L. Medintz, E. Stratakis, W. J. Parak and A. G. Kanaras, *Chem. Rev.*, 2019, **119**, 4819–4880.
15 X. Chen, L. Zhou, Z. Guo and Q. Song, *Mater. Adv.*, 2024, **5**, 1332–1339.
16 W. Wang, X. Chen and S. Efrima, *J. Phys. Chem. B*, 1999, **103**, 7238–7246.
17 N. Ukah and H. A. Wegner, *Nanoscale*, 2024, **16**, 18524–18533.
18 E. L. Albright, T. I. Levchenko, V. K. Kulkarni, A. I. Sullivan, J. F. DeJesus, S. Malola, S. Takano, M. Nambo, K. Stamplecoskie, H. Häkkinen, T. Tsukuda and C. M. Crudden, *J. Am. Chem. Soc.*, 2024, **146**, 5759–5780.
19 I. T. Pulido-Díaz, A. Serrano-Maldonado, C. C. López-Suárez, P. A. Méndez-Ocampo, B. Portales-Martínez, A. Gutiérrez-Alejandre, K. P. Salas-Martin and I. Guerrero-Ríos, *Dalton Trans.*, 2021, **50**, 3289–3298.
20 J. Hu, Z. Chen, M. Li, X. Zhou and H. Lu, *ACS Appl. Mater. Interfaces*, 2014, **6**, 13191–13200.
21 R. Ren, S. Li, J. Li, J. Ma, H. Liu and J. Ma, *Catal. Sci. Technol.*, 2015, **5**, 2149–2156.
22 M. Cargnello, N. L. Wieder, P. Canton, T. Montini, G. Giambastiani, A. Benedetti, R. J. Gorte and P. A. Fornasiero, *Chem. Mater.*, 2011, **23**, 3961–3969.
23 S. Koh, W. D. Kim, W. K. Bae, Y. K. Lee and D. C. Lee, *Chem. Mater.*, 2019, **31**, 1990–2001.
24 P. M. Shem, R. Sardar and J. S. Shumaker-Parry, *Langmuir*, 2009, **25**, 13279–13283.
25 G. Schmid, R. Pfeil, R. Boese, F. Bandermann, S. Meyer, G. H. M. Calis and J. W. A. van der Velden, *Chem. Ber.*, 1981, **114**, 3634–3642.
26 C. Tang, K. H. Ku, S. X. L. Luo, A. Concellón, Y. C. M. Wu, R. Q. Lu and T. M. Swager, *ACS Nano*, 2020, **14**, 11605–11612.
27 X. Yao, M. Jin, J. Du and D. Wan, *ACS Appl. Nano Mater.*, 2023, **6**, 6653–6661.
28 D. Sahu and P. Das, *RSC Adv.*, 2015, **5**, 3512–3520.
29 M. A. S. Garcia, M. Ibrahim, J. C. S. Costa, P. Corio, E. V. Gusevskaya, E. N. dos Santos, K. Philippot and L. M. Rossi, *Appl. Catal., A*, 2017, **548**, 136–142.
30 Z. Li, J. Li, J. Liu, Z. Zhao, C. Xia and F. Li, *ChemCatChem*, 2014, **6**, 1333–1339.
31 S. Zhu, Z. Lv, X. Jia, J. Wang, X. Li, M. Dong and W. Fan, *Appl. Catal., B*, 2024, **351**, 123958.
32 X. Quan, S. Kerdphon, B. B. C. Peters, J. Rujirawanich, S. Krajangsri, J. Jongcharoenkamol and P. G. Andersson, *Chem. – Eur. J.*, 2020, **26**, 13311–13316.
33 S. R. Lee, N. Bhuvanesh and O. V. Ozerov, *Inorg. Chem.*, 2024, **63**, 24133–24140.
34 M. Valero, D. Bouzouita, A. Palazzolo, J. Atzrodt, C. Dugave, S. Tricard, S. Feuillastre, G. Pieters, B. Chaudret and V. Derdau, *Angew. Chemie.*, 2020, **132**, 3545–3550.

35 W. Oberhauser, C. Evangelisti, A. Liscio, A. Kovtun, Y. Cao and F. Vizza, *J. Catal.*, 2018, **368**, 298–305.
36 D. Xu, P. Diao, T. Jin, Q. Wu, X. Liu, X. Guo, H. Gong, F. Li, M. Xiang and Y. Ronghai, *ACS Appl. Mater. Interfaces*, 2015, **7**, 16738–16749.
37 R. H. Crabtree, *Chem. Rev.*, 2017, **117**, 9228–9246.
38 M. Trincado, J. Bösken and H. Grützmacher, *Coord. Chem. Rev.*, 2021, **443**, 213967.
39 E. Balaraman, E. Khaskin, G. Leitus and D. Milstein, *Nat. Chem.*, 2013, **5**, 122–125.
40 B. Gogoi, P. Borgohain, S. G. Patra, B. J. Borah and P. Das, *Organometallics*, 2024, **43**, 2002–2015.
41 T. Mori, C. Ishii and M. Kimura, *Org. Process Res. Dev.*, 2019, **23**, 1709–1717.
42 V. Cherepakhin and T. J. Williams, *ACS Catal.*, 2018, **8**, 3754–3763.
43 R. Kawahara, K. Fujita and R. Yamaguchi, *J. Am. Chem. Soc.*, 2012, **134**, 3643–3646.
44 D. Borah, B. Saha, B. Sarma and P. Das, *Dalton Trans.*, 2020, **49**, 16866–16876.
45 M. K. Awasthi and S. K. Singh, *Inorg. Chem.*, 2019, **58**, 14912–14923.
46 H. M. Liu, L. Jian, C. Li, C. C. Zhang, H. Y. Fu, X. L. Zheng, H. Chen and R. X. Li, *J. Org. Chem.*, 2019, **84**, 9151–9160.
47 A. Sarbajna, I. Dutta, P. Daw, S. Dinda, S. M. W. Rahaman, A. Sarkar and J. K. Bera, *ACS Catal.*, 2017, **7**, 2786–2790.
48 D. R. Pradhan, S. Pattanaik, J. Kishore and C. Gunanathan, *Org. Lett.*, 2020, **22**, 1852–1857.
49 Z. Dai, Q. Luo, H. Jiang, Q. Luo, H. Li, J. Zhang and T. Peng, *Catal. Sci. Technol.*, 2017, **7**, 2506–2511.
50 Z. Shao, Y. Wang, Y. Liu, Q. Wang, X. Fu and Q. Liu, *Org. Chem. Front.*, 2018, **5**, 1248–1256.
51 Y. Sawama, K. Morita, S. Asai, M. Kozawa, S. Tadokoro, J. Nakajima, Y. Monguchi and H. Sajiki, *Adv. Synth. Catal.*, 2015, **357**, 1205–1210.
52 K. Bordoloi, G. D. Kalita and P. Das, *Dalton Trans.*, 2022, **51**, 9922–9934.
53 K. Bordoloi, G. D. Kalita and P. Das, *ACS Appl. Nano Mater.*, 2023, **6**, 14786–14797.
54 B. Lakshminarayana, M. Selvaraj, G. Satyanarayana and C. Subrahmanyam, *Catal. Rev. - Sci. Eng.*, 2024, **66**, 259–342.
55 K. Li, R. Qin, K. Liu, W. Zhou, N. Liu, Y. Zhang, S. Liu, J. Chen, G. Fu and N. Zheng, *ACS Appl. Mater. Interfaces*, 2021, **13**, 52193–52201.
56 T. Lu, J. Lin, X. Liu, X. Wang and T. Zhang, *Langmuir*, 2016, **32**, 2771–2779.
57 F. Cárdenas-Lizana, Y. Hao, M. Crespo-Quesada, I. Yuranov, X. Wang, M. A. Keane and L. Kiwi-Minsker, *ACS Catal.*, 2013, **3**, 1386–1396.
58 B. K. Koç, G. Yıldız, S. Can, İ. H. Patir and Ö. Metin, *J. Catal.*, 2025, **443**, 115974.
59 J. Lyu, J. Wang, C. Lu, L. Ma, Q. Zhang, X. He and X. Li, *J. Phys. Chem. C*, 2014, **118**, 2594–2601.
60 Z. Hu, Y. Cheng, M. Wu, Y. Duan, Y. Yang and T. Lu, *Catalysts*, 2023, **13**, 1438.
61 M. Zhang, Q. Zhang, Y. Lu, Y. Zhao, D. Zhang and T. Huang, *ACS Appl. Nano Mater.*, 2021, **4**, 13995–14003.
62 D. Bhattacherjee, Shaifali, A. Kumar, G. V. Zyryanov and P. Das, *Mol. Catal.*, 2021, **514**, 111836.
63 F. Leng, I. C. Gerber, P. Lecante, S. Moldovan, M. Girleanu, M. R. Axet and P. Serp, *ACS Catal.*, 2016, **6**, 6018–6024.
64 I. Dutta, A. Sarbajna, P. Pandey, S. M. W. Rahaman, K. Singh and J. K. Bera, *Organometallics*, 2016, **35**, 1505–1513.
65 C. B. García-Reyes, J. J. Salazar-Rábago, M. S. Polo and V. C. Ramos, *Catalysts*, 2022, **12**, 1341.
66 J. Y. Zhu, Q. Xue, Y. Y. Xue, Y. Ding, F. M. Li, P. Jin, P. Chen and Y. Chen, *ACS Appl. Mater. Interfaces*, 2020, **12**, 14064–14070.
67 S. Siracusano, V. Baglio, S. A. Grigoriev, L. Merlo, V. N. Fateev and A. S. Aricò, *J. Power Sources*, 2017, **366**, 105–114.
68 Y. Sugita, T. Tamaki, H. Kuroki and T. Yamaguchi, *Nanoscale Adv.*, 2020, **2**, 171–175.
69 G. Jin, J. Liu, C. Wang, W. Gu, G. Ran, B. Liu and Q. Song, *Appl. Catal., B*, 2020, **267**, 118725.
70 H. Wang, M. Ming, M. Hu, C. Xu, Y. Wang, Y. Zhang, D. Gao, J. Bi, G. Fan and J. S. Hu, *ACS Appl. Mater. Interfaces*, 2018, **10**, 22340–22347.
71 J. Quinson, *Adv. Colloid Interface Sci.*, 2022, **303**, 102643.
72 A. Dolgov, D. Lopaev, C. J. Lee, E. Zoethout, V. Medvedev, O. Yakushev and F. Bijkerk, *Appl. Surf. Sci.*, 2015, **353**, 708–713.
73 P. Salimi and M. M. Najafpour, *Chem. – Eur. J.*, 2020, **26**, 17063–17068.
74 L. Schick, R. Sanchis, V. González-Alfaro, S. Agouram, J. M. López, L. Torrente-Murciano, T. García and B. Solsona, *Chem. Eng. J.*, 2019, **366**, 100–111.
75 E. Yazdani and A. Heydari, *J. Organomet. Chem.*, 2020, **924**, 121453.
76 H. G. Ghalehshahi and R. Madsen, *Chem. – Eur. J.*, 2017, **23**, 11920–11926.
77 Q. Yan, X. Wu, H. Jiang, H. Wang, F. Xu, H. Li, H. Zhang and S. Yang, *Coord. Chem. Rev.*, 2024, **502**, 215622.
78 Y. Zhang, Y. Zhou, D. Sun, Y. Nie, D. Wu, L. Ban, B. Tang, S. Yang, H. Li, T. Ma and H. Zhang, *Coord. Chem. Rev.*, 2025, **527**, 216395.
79 H. Tian, A. Wang, H. Pan, H. Zhang and S. Yang, *Ind. Crops Prod.*, 2024, **222**, 119738.
80 L. Chen, Y. Liu, H. Zhang, Y. Li, S. Zhang, Y. Hu, H. Li and S. Yang, *React. Chem. Eng.*, 2023, **8**, 1464–1475.
81 M. Schalk, F. Cabello-Hurtado, M. A. Pierrel, R. Atanossova, P. Saindrenan and D. Werck-Reichhart, *Plant Physiol.*, 1998, **118**, 209–218.
82 Y. X. Si, S. Ji, N. Y. Fang, W. Wang, J. M. Yang, G. Y. Qian, Y. D. Park, J. Lee and S. J. Yin, *Process Biochem.*, 2013, **48**, 1706–1714.
83 Z. Chen, J. Hang, S. Zhang, Y. Yuan, F. Verpoort and C. Chen, *Catalysts*, 2023, **13**, 1225.
84 Y. Sawama, K. Morita, T. Yamada, S. Nagata, Y. Yabe, Y. Monguchi and H. Sajiki, *Green Chem.*, 2014, **16**, 3439–3443.

85 W. I. Lone, A. Rashid, B. A. Bhat and S. Rashid, *Chem. Commun.*, 2024, **60**, 6544–6547.
86 C. V. Rode and R. V. Chaudhari, *Ind. Eng. Chem. Res.*, 1994, **33**, 1645–1653.
87 A. H. Pizarro, C. B. Molina, J. A. Casas and J. J. Rodriguez, *Appl. Catal., B*, 2014, **158–159**, 175–181.
88 F. Cárdenas-Lizana, S. Gómez-Quero, A. Hugon, L. Delannoy, C. Louis and M. A. Keane, *J. Catal.*, 2009, **262**, 235–243.
89 P. Balasubramanian, T. S. T. Balamurugan, S. M. Chen and T. W. Chen, *J. Hazard. Mater.*, 2019, **361**, 123–133.
90 D. Balram, K. Y. Lian and N. Sebastian, *Ultrason. Sonochem.*, 2020, **60**, 104798.
91 X. Wang, N. Perret and M. A. Keane, *Chem. Eng. J.*, 2012, **210**, 103–113.
92 M. Ebadi, N. Asikin-Mijan, M. S. Md. Jamil, A. Iqbal, E. Yousif, A. R. Md. Zain, T. H. T. Aziz and M. R. Yusop, *Polymers*, 2023, **15**, 232.